PCCP

PERSPECTIVE

View Article Online
View Journal | View Issue

Cite this: *Phys. Chem. Chem. Phys.*, 2025, **27**, 6408

Liquid crystals as solid-state templates

Nurjahan Khatun,[a] Agnes C. Nkele[b] and Kushal Bagchi*[a]

Received 28th November 2024,
Accepted 7th March 2025

DOI: 10.1039/d4cp04526b

rsc.li/pccp

Liquid crystals (LCs) combine the anisotropy of crystals with the fast molecular dynamics of liquids. Controlling the molecular orientation of LCs is the key enabling feature of liquid crystal displays (LCDs), a technology that has played a pivotal role in ushering in the digital age of today. Here we review controlling molecular organization in LCs over large distances for a different application: the assembly of macroscopically organized solids. The traditional approach of controlling orientational order in organic solids is growing single crystals, a process limited by slow kinetics. In this article, we review an alternate approach: the generation of organized solids through the (i) polymerization, (ii) physical gelation, and (iii) vitrification of small-molecule LCs. The generation of solids through these routes is enabled by innovations in (i) molecular design, (ii) formulation chemistry, and (iii) macroscopic alignment of LCs. Controlling molecular orientation, defects, and deformations in the precursor LC phase enables the assembly of solids with unique properties such as programmable responses to stimuli. We discuss the "organize and solidify" approach for the preparation of materials with LC order for soft robotics, chemical sensing, and lithographic patterning. Finally, we outline future challenges and opportunities in the field of liquid crystalline solids.

I. Introduction

Control of atomic and molecular organization over macroscopic distances is central to the advancement of science and technology. The growth of "human-sized" single crystalline silicon ingots, through processes like the Czochralski method, is one of the first steps in the manufacture of computer chips. Growing large single crystals, however, is an appropriate route for macroscopic control of microstructure in materials that crystallize fast. Single-component metals like nickel and inorganic semiconductors like silicon are examples of materials that belong to this class. Crystal growth of metals[1] and inorganic semiconductors[2] from their melts can occur at velocities between 1 and 100 m s^{-1}. Several functional molecular and polymeric crystals, however, exhibit growth velocities that are several orders of magnitude slower. The drug molecule indomethacin exhibits a maximum crystal growth velocity of $\sim 10^{-6}$ m s^{-1} from its supercooled liquid state.[3] Similarly, crystals of multifunctional polymer polyethylene oxide (PEO) grow at a maximum velocity of $\sim 10^{-4}$ m s^{-1} from the melt.[4] The slow crystallization of organic systems is linked to their large entropies of fusion.[5]

Slow crystallization kinetics necessitates an alternate paradigm to single crystal growth for the macroscopic control of microstructure in both molecular and polymeric solids. A key motivation for controlling molecular organization is to impart anisotropy. Introducing long range orientational anisotropy in organic materials can serve diverse purposes, from improving electronic and ionic transport[6] to increasing moduli.[7] The development of a fast and scalable method to combine liquid crystalline orientational anisotropy with the mechanical robustness of the solid state could lead to new applications as well as improved performance of existing technologies that use organic solids. Molecular solids are widely used in pharmacology[8,9] and organic electronics.[10–16] Synthetic polymeric solids are ubiquitous in the commodities and technologies of the modern world, from the Nylon in toothbrush bristles to the Kapton on the James Webb telescope. Rendering new properties and functionalities to organic solids through macroscopic control of molecular organization could therefore have far-reaching societal implications.

The topic of the article, the directed self-assembly and subsequent solidification of LCs, allows for controlling nanoscale order over macroscopic volumes in organic materials. Sections II and III of the article are introductory and provide background understanding for subsequent parts while Sections IV–VIII deal with the main focus of the article. A reader familiar with LCs can begin directly in Section IV. Starting from this section we discuss how liquid crystalline order and alignment can be transferred both to solid-like materials such as elastomers (Section V) and physical gels (Section VI) as well as true solids like liquid crystal networks (Section V) and molecular glasses (Section VII). When liquid crystalline order is

[a] *Department of Chemistry, Rice University, Houston, TX 77005, USA. E-mail: kb122@rice.edu*
[b] *Applied Physics Program, Smalley-Curl Institute, Rice University, Houston, TX 77005, USA*

transferred to gels and elastomers, the long-range orientational order of molecular single crystals can be combined with the responsiveness and stretchability of polymeric gels[17] and rubbery polymers.[18,19] Across the article, we review the potential that solids derived from LCs hold for fields such as photonics and patterning. Finally, in Section VIII we discuss future challenges and opportunities in the field of liquid crystalline solids.

II. A brief overview of the physics and chemistry of liquid crystals

What are LCs?

LCs are phases of matter that combine the molecular mobility of liquids with the anisotropy of the crystalline state. LCs wherein the phase behavior is determined by temperature are called thermotropic LCs and are the central focus of the present article. Thermotropic liquid crystalline phases are observed for molecules that exhibit anisotropic shapes. Rod-, disc-, and banana-shaped molecules are common thermotropic liquid crystal formers. LC phases are also observed in solutions of surfactants that assemble into anisotropic structures such as cylinders. Additionally, LC phases are observed in sufficiently concentrated solutions of anisotropic particles such as semiconductor nanorods[20] and carbon nanotubes[21] or biomolecules such as DNA.[22] In these LCs, called lyotropic LCs, phase behavior is determined by both concentration and temperature.

First discovered towards the end of the nineteenth century by Austrian botanist Friedrich Reinitzer, LCs have continued to be a theme of research interest owing to the prominent role they play in modern technology. LCs are widely used in display technology, where the ability to control and switch molecular orientation is used to alter the transmission of light, and thereby turn pixels on and off. It is estimated that $\sim$100 million liquid crystal display (LCD) televisions are sold annually. LCs are also widely used in adaptive optics[23] and spatial light modulators.[24] Optical changes produced by the response of liquid crystals to analytes have been used to sense endotoxins,[25] toxic gases,[26] and heavy metal ions.[27] Here, we discuss leveraging the properties of LCs for the synthesis of macroscopically structured organic solids. Below we provide a brief introduction to the physics and chemistry of LCs for readers less familiar with these materials. In the subsequent section, we describe the macroscopic alignment of LCs. Experts in LCs and their alignment can move directly to Section IV.

Structure and dynamics in different LC phases

The nematic phase is the simplest LC state. As shown in Fig. 1, a nematic LC is an orientationally ordered fluid. Both calamitic (or rod-shaped) and discotic (or disk-shaped) mesogens exhibit nematic phases. Orientational anisotropy in nematic LCs gives rise to optical birefringence. The texture of nematic LCs is therefore easily visualized under a polarized optical microscope (POM). Unlike more structured LC phases, nematics exhibit no translational order. Consequently, nematics are more fluid than other LC phases. The diffusion coefficient of canonical nematic liquid crystal former, 5CB, whose molecular structure is shown in Fig. 1, is $\sim 10^{-11}$ m^2 s^{-1} in the nematic phase. This is only two orders of magnitude smaller than the diffusion coefficient of water at room temperature.

The amount of nematic ordering in a material can be quantified using the orientational order parameter, S_z. which is a second order Legendre polynomial and is given by the equation:

$$S_z = \frac{3\langle \cos^2\theta \rangle - 1}{2} \quad (1)$$

where, θ is the angle between the molecular long axis and the surface normal. When the molecular long axis is aligned perfectly parallel to the surface normal, $\theta = 0^\circ$ and $S_z = 1$. On the other hand, when the molecular long axis is perpendicular to the surface normal, $\theta = 90^\circ$ and $S_z = -1/2$. In an orientationally isotropic material, $\langle \cos^2\theta \rangle = 1/3$, resulting in $S_z = 0$. The nematic order parameter can be determined using NMR, UV-VIS, Raman, infrared, and dielectric spectroscopy and optical birefringence measurements.[28–30]

There is a rich diversity of liquid crystalline phases that exhibit both orientational and translational order. As shown in Fig. 1, both in the smectic phase, formed from calamitic mesogens and in the columnar hexagonal phase, formed from discotic mesogens; there is an ordering of the molecular center of masses. In smectic LCs, as shown in Fig. 1, molecules organize into layers. In columnar phases, molecules organize into columns, which in turn are typically organized into hexagonal or rectangular lattices. The diffusion coefficient of 8CB, a canonical smectic liquid crystal former is $\sim 10^{-11}$ m^2 s^{-1} in the smectic phase. HAT5, which forms columnar hexagonal phases, exhibits a diffusion coefficient of $\sim 10^{-14}$ m^2 s^{-1} in its liquid crystalline phase. The columnar hexagonal phase exhibits much slower dynamics but a greater degree of translational order than that seen in nematic and smectic LC phases.

Once the diffusion coefficient becomes smaller than $\sim 10^{-20}$ m^2 s^{-1}, the material, on all practical timescales is a solid. As is evident from Table 1, which lists diffusion coefficients of a variety of non-crystalline materials, the dynamics of most common LCs are much closer to water than a glassy solid. The molecular dynamics of LCs, however, are known only for a few select molecules, with most of the literature focusing on structure. Consequently, lots of materials are identified to be LCs purely based on structural measurements like polarized optical microscopy and X-ray scattering. We caution readers against this approach. To truly be a liquid crystal, a material must exhibit liquid-like dynamics. The diffusion coefficient of a liquid crystal must be greater than 10^{-20} m^2 s^{-1}. As we discuss throughout this article, solids can have liquid crystalline order but these materials are distinct dynamically and mechanically from true, fluid LCs like 5CB, 8CB, and HAT5.

Introducing chirality into LCs provides access to entirely new structures and phases. The simplest chiral phase, the cholesteric or chiral nematic phase is shown in Fig. 1. In the

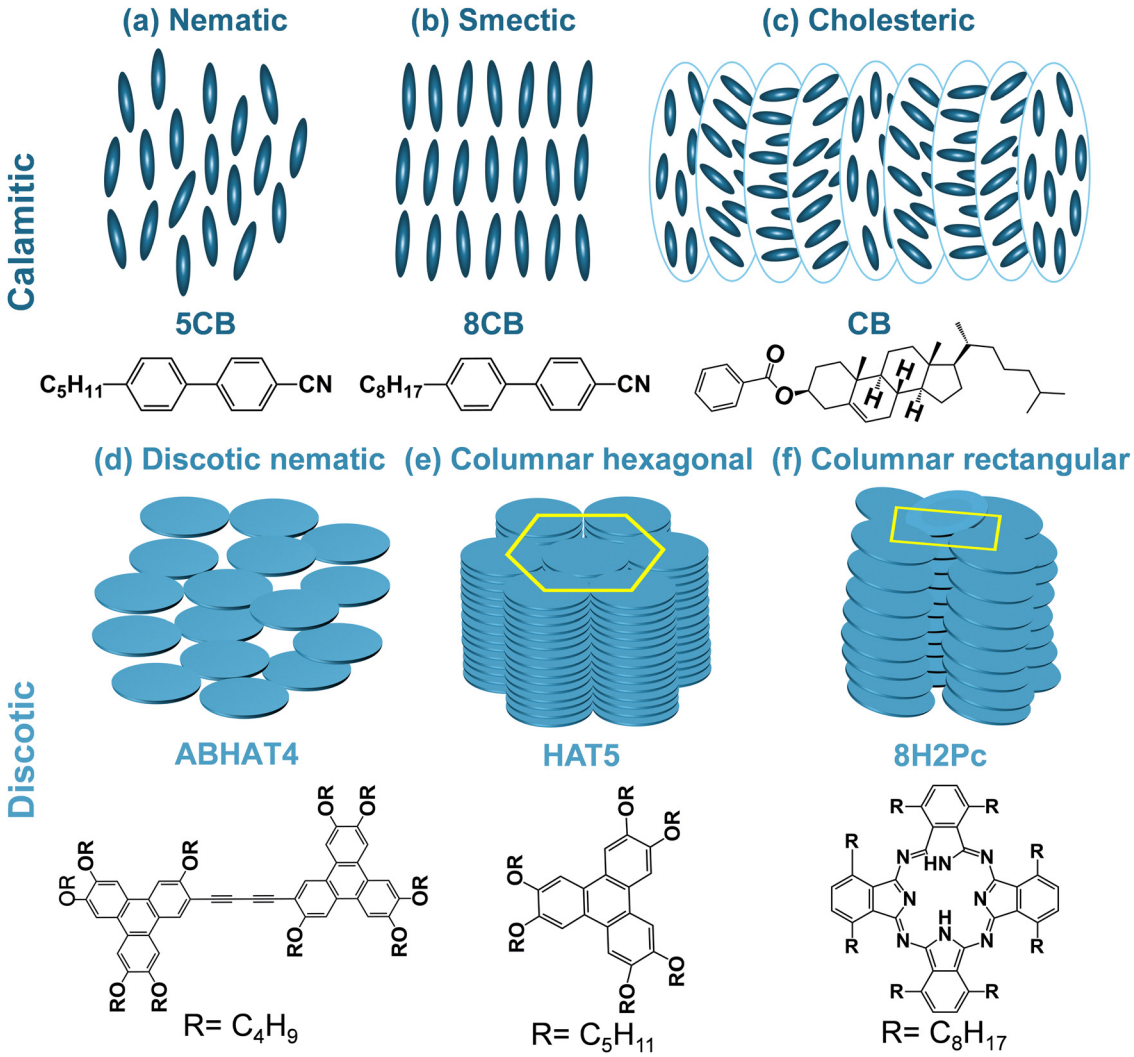

Fig. 1 Organization in calamitic (a)–(c) and discotic (d)–(f) liquid crystalline phases with molecular structure. Calamitic and discotic refer to molecules with rod-like and disk-like shapes, respectively. Molecular anisotropy is a pre-requisite for the formation of thermotropic liquid crystalline phases. The chemical names for 5CB in (a), 8CB in (b), CB in (c), ABHAT4 in (d), HAT5 in (e), and 8H_2Pc in (f) are 4-*n*-pentyl-4′-cyanobiphenyl, 4-octyl-4′-cyanobiphenyl, 5-cholesten-3-yl benzoate,1,4-bis(3,6,7,10,11-pentabutoxytriphenylen-2-yl)buta-1,3-diyne, 2,3,6,7,10,11-hexakis(pentyloxy)triphenylene and 1,4,8,11,15,18,22,25-octaoctylphthalocyanine, respectively.

Table 1 Diffusion coefficients of molecules in liquid, liquid crystalline, and glassy phases. We list the order of magnitude of the diffusion coefficient in each case. For LCs, diffusion coefficients can be anisotropic. However, in-plane and out-of-plane diffusion coefficients typically are of the same order of magnitude

Molecule, phase	Diffusion coefficient (m^2 s^{-1}) (temperature (K))	Ref.
Water, isotropic liquid	10^{-9} (298 K)	31
5CB, nematic LC	10^{-11} (300 K)	32
8CB, smectic LC	10^{-11} (304 K)	32
HAT5, columnar hexagonal LC	10^{-14} (380 K)	33
Indomethacin, glassy solid	10^{-20} (315 K)	34

chiral nematic phase, the director twists to form helicoidal structure wherein the screw axis is perpendicular to the molecular long axis. The distance over which the molecular long axis executes a 360° rotation is known as the pitch. Chirality is usually imparted to LC phases through the doping of a chiral molecule. The concentration of the chiral molecule and its helical twisting power determine the pitch of the LC phase. Mesogens, like the one shown in Fig. 1c, can be chiral themselves. In both cases, chiral phases occur but the former offers greater tunability. For instance, in mixtures of chiral and achiral molecules, a whole range of pitches can be selected by tuning composition, whereas for a single-component system only a single pitch is possible (at a fixed temperature).

Chiral LC states can exhibit much more complex structures than the cholesteric phase discussed earlier. Discotic and smectic LCs also exhibit chiral phases. In highly chiral systems, three-dimensional cubic structures, called blue-phases occur.[35–41] A full discussion of all the different liquid crystalline chiral phases is beyond the scope of the present

manuscript and we direct the interested reader to relevant articles.[42] We will, however, discuss the use of chiral phases, like the blue-phase, to assemble functional organic solids.

Defects in LCs

In condensed matter, where there is structure and order, there are also defects. LCs are no different and exhibit a range of defects. While defects in crystalline solids are described in terms of positional order, in LCs defects are defined with respect to orientational order. Of particular interest are topological defects in LCs, which as discussed in the Section V can be controllably introduced to program material response to stimuli.

Mathematically, topological defects are defined as singularities in the director field. Topological defects occur when the molecular orientation varies in space in such a manner as to give rise to local isotropic regions. Topological defects lie at the core of these isotropic regions. Examples of topological defects are shown in Fig. 2a. As shown in the figure, a topological defect has associated with it both magnitude and sign. The magnitude specifies the number of rotations the director field executes around the center of the defect. For instance, the director field rotates 360° around a +1 defect (Fig. 2). Topological defects exhibit analogous behavior to point charges. Like the net charge over sufficiently large sample volumes is necessarily zero, the sum of topological defects over large enough spaces is also zero. The sign of a topological defect helps identify defects that cancel each other out. When topological defects of the same magnitude and opposite sign come in contact, they annihilate.

Elasticity in LCs

Elastic properties play a central role in determining the behavior of LCs. The bulk organization in LCs is often determined by minimizing elastic free energy which in turn is dictated by the confining surfaces (in applications and in laboratory studies LCs are often sandwiched between two inorganic surfaces). For simple and complex liquid crystalline phases alike, a given molecular organization is often adopted on a certain surface because it minimizes the bulk elastic free energy.[40]

Different LC phases exhibit differing kinds and magnitudes of deformation modes. A nematic liquid crystal exhibits three deformation modes: splay, twist, and bend. For thermotropic nematic LCs, the elastic constant for each of these different modes is ~10 pN. Splay, twist and bend deformation modes are shown in Fig. 2b. The elastic constants corresponding to splay, twist, and bend deformations are denoted as K_{11}, K_{22}, and K_{33}, respectively, while $\boldsymbol{n}$ is the director. The elastic free energy (F) density can be expressed as follows:

$$F = \frac{1}{2}\left\{K_{11}(\nabla \cdot \boldsymbol{n})^2 + K_{22}(\boldsymbol{n} \cdot \nabla \times \boldsymbol{n})^2 + K_{33}[\boldsymbol{n} \times (\nabla \times \boldsymbol{n})]^2\right\} \quad (2)$$

For thermotropic nematic LCs like 5CB, the splay, bend, and twist elastic constants are approximately equal. For lyotropic LCs like water-based chromonic phases, the twist modulus is substantially lower than splay and bend.[43] The elastic anisotropy of chromonic LCs gives rise to new physics.[44] For instance, due to a small twist-elastic constant, chromonic LCs composed of achiral mesogens easily form chiral structures upon flow.[44] Thermotropic smectic LCs exhibit splay deformation but do not exhibit twist and bend modes[45,46]

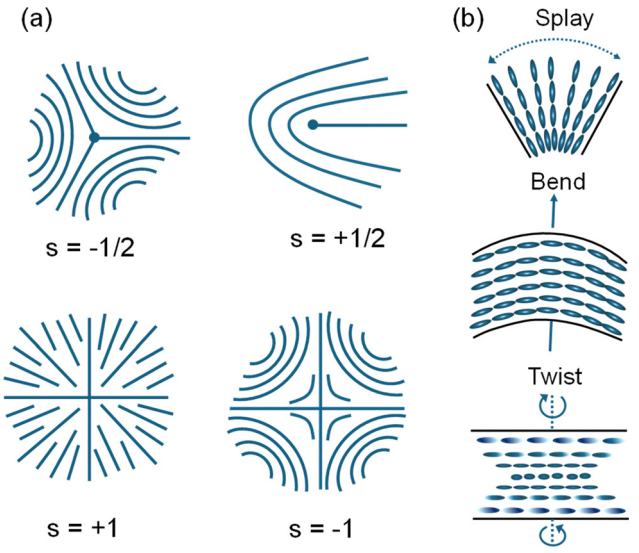

Fig. 2 Defects (a) and deformation modes (b) in nematic LCs.

III. Macroscopic alignment of liquid crystals

One of the primary advantages of LCs is that they can be aligned over macroscopic distances. The general strategies to organize LCs in the bulk are (1) control of surface chemistry, (2) control of surface topology, and (3) the application of electrical and magnetic fields. We discuss below each of these approaches briefly.

Surface chemistry

LC organization is exquisitely sensitive to surface chemistry. When confined between common inorganic surfaces like silicate glass and in the nematic phase, mesogens typically orient with the molecular long axis perpendicular to the surface normal. In such cases, the molecular orientation is random in the plane and the anchoring is known as planar degenerate (Fig. 3a). A common strategy to induce vertical organization of the molecular long axis or homeotropic anchoring in nematic mesogens is through the grafting of self-assembled monolayers of small-molecules and polymers. Adding a single layer of silane molecules to glass surfaces causes the anchoring throughout micron thick cells to become homeotropic (Fig. 3b). Nanometer level changes in surface chemistry influence the structure of nematic LCs over microns.

The nature of surface chemical modifications required for inducing alignment varies with the complexity of the liquid crystalline phase. As discussed above, for nematic LCs, grafting a single monolayer is often sufficient to induce homeotropic

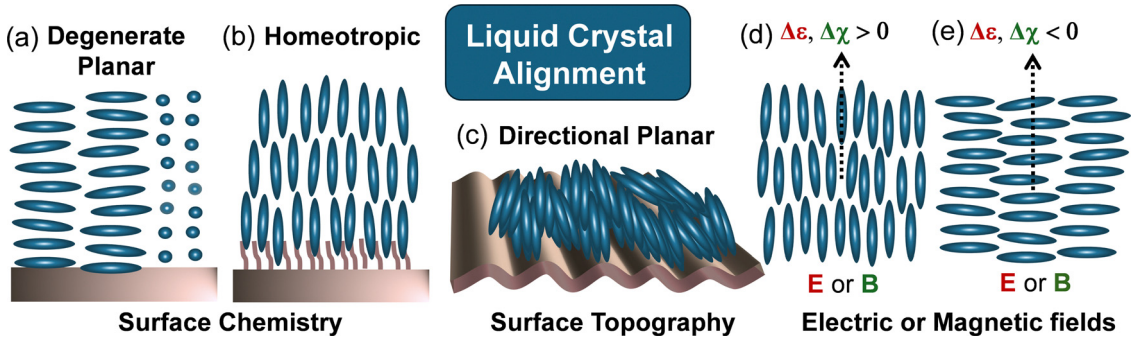

Fig. 3 Alignment of liquid crystals using surface chemistry (a) and (b), surface topography (c) and electric or magnetic fields (d) and (e). (a) Depicts the degenerate planar organization typically adopted on untreated inorganic surfaces while shown in (b) is the inducement of homeotropic alignment in a calamitic liquid crystal through grafting a self-assembled monolayer. Depicted in (c) is the induction of directional planar alignment through the introduction of grooves on a surface. (d) Depicts controlling molecular organization through the application of electric (E) or magnetic (B) field in materials with positive dielectric anisotropy, $\Delta\varepsilon$, or positive susceptibility anisotropy, $\Delta\chi$. (e) depicts the same when these quantities are negative.

alignment. In blue-phase liquid crystals, wherein millions of molecules organize into ~100 nm sized cubic lattices, lithographically defined chemical patterns are used to induce uniform lattice orientation. These patterns consist of alternating regions of silicon and a polymer brush (or siliane) which induce planar and homeotropic alignment, respectively. In these patterns, the chemistry varies spatially with a period that is related to the blue phase lattice size.[40,47]

Surface topography

The bulk structure of nematic LCs is sensitive to nanoscale topographical features. Grooved surfaces are often used to induce directional planar alignment of LCs as shown in Fig. 3c. In calamitic phases, like the nematic or the smectic C phases, orientation of the molecular long axis along the grooves is driven by the minimization of elastic free energy.[48] Common methods to create grooved surfaces include Glancing angle deposition (GLAD) of thin metal films[49] and rubbing polymer films. Although rubbing does generate grooved surfaces and induce directional planar alignment, it is controversial whether the topography induces alignment or whether the organization is a result of chain alignment induced in the polymeric substrate due to rubbing.[50]

Substrates with micropatterned topography are used to align more complex liquid crystalline phases like columnar hexagonal[51,52] and lyotropic chromonic[53] LCs.

Electric and magnetic fields

Both electric and magnetic fields can be used to align LCs. Electric field alignment is employed to create homeotropic alignment of nematic phases in LCD displays. Homeotropic alignment prevents transmission of LED backlight and thereby creates the off state in these devices. Molecular orientation in calamitic nematic LCs in the presence of an electric field depends on whether the dielectric anisotropy, $\Delta\varepsilon$, is positive or negative. In calamitic mesogens with a positive dielectric anisotropy, like 5CB, the molecular long axis aligns along the direction of the electric field. The opposite effect is observed in materials with a negative dielectric anisotropy, where the molecular long axis adopts a perpendicular orientation with respect to the applied electric field.

The threshold electric field, E_c, the value above which the molecular orientation in a LC responds to an applied electric field is given by the equation:

$$E_c = \left(\frac{\pi}{d}\right)\left(\frac{K}{\varepsilon_0 \Delta\varepsilon}\right)^{1/2} \quad (3)$$

where, ε_0 is the vacuum permittivity, K is an elastic constant, $\Delta\varepsilon$ is the dielectric anisotropy, and d is the thickness.[54]

For magnetic field alignment, anisotropy in diamagnetic susceptibility, referred to henceforth as the susceptibility anisotropy, plays an analogous role to that played by dielectric anisotropy during electric field alignment. Calamitic mesogens with positive and negative susceptibility anisotropy align with their molecular long axes parallel and perpendicular to the applied magnetic field vector, respectively.

The threshold magnetic field (B_c), the magnetic equivalent of the threshold electric field defined above, can be expressed mathematically as:

$$B_c = \left(\frac{\pi}{d}\right)\left(\frac{K}{\mu_0 \Delta\chi}\right)^{1/2} \quad (4)$$

where, μ_0 is permeability of vacuum, $\Delta\chi$ is the susceptibility anisotropy, K is an elastic constant, and d is the thickness.[55]

IV. Solidification of liquid crystals

Liquid crystalline order can be transferred to the solid state through polymerization, gelation, and vitrification. We discuss each of these methods in the subsequent sections of the article. Before we delve into the synthesis of liquid crystalline solids and their applications in technology, we discuss below the characteristics that set these materials apart from conventional crystalline solids. We also discuss the broad range of elastic properties they can exhibit.

The term "liquid crystalline solid," at first glance, might seem like an oxymoron. These solids, however, are distinct from both conventional liquids and crystalline solids. Unlike

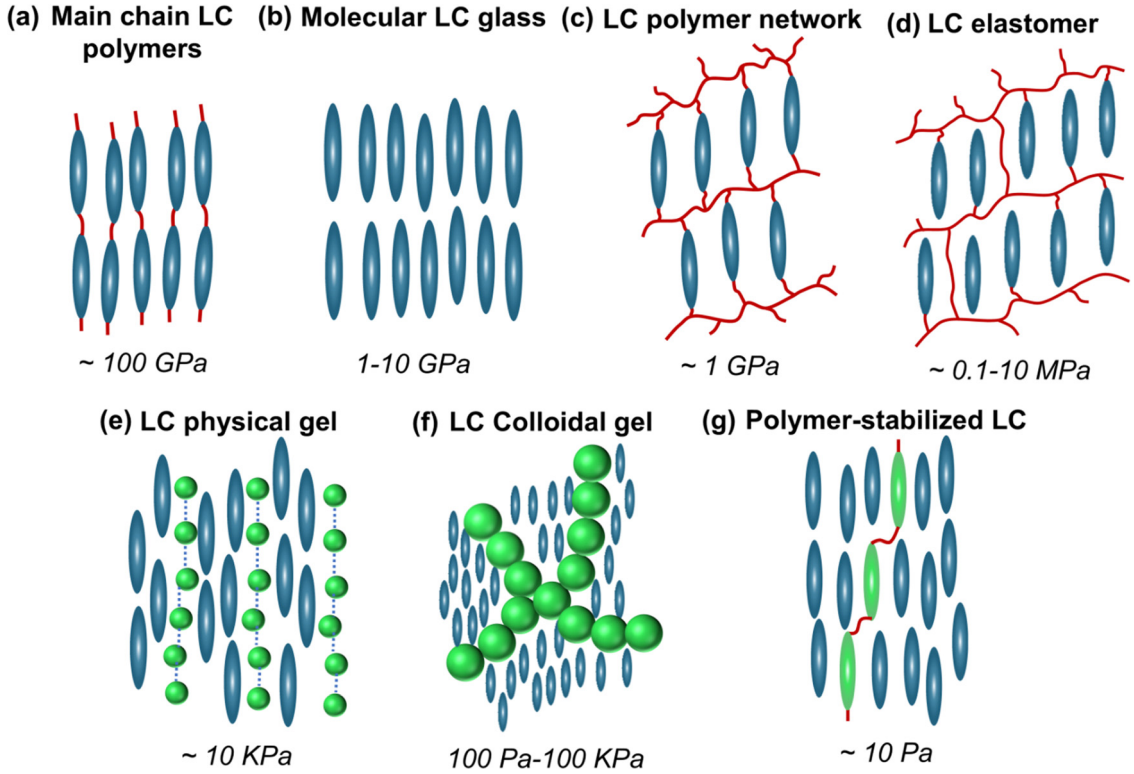

Fig. 4 Molecular organization and moduli of liquid crystalline solids. The solids are organized in descending order of stiffness, with main chain liquid crystal polymers (a) being the stiffest and polymer stabilized liquid crystals (g) being the softest. Covalent bonds are shown in red in (a), (c), (d) and (g). Non-covalent bonds or weak interactions are shown through doted blue lines in liquid crystalline physical gels (e). The large spheres in (f) represent a colloidal particle in a liquid crystal solvent.

crystals, liquid crystalline solids do not exhibit long range translational order in three dimensions. At the same time, liquid crystalline solids do not exhibit the fast dynamics or mechanical response of liquids. All liquid crystalline solids exhibit a Young's or elastic modulus, one of the defining properties of solids. There are many kinds of liquid crystalline solids, and many routes to produce them. The different kinds of liquid crystalline solids are shown in Fig. 4. As shown in the figure, liquid crystalline solids vary from being amongst the stiffest to the softest of materials.

The objective of the article is not to review all kinds of liquid crystalline solids but rather to focus on those systems that can be macroscopically aligned in their precursor liquid state prior to solidification. We do not focus on main-chain liquid crystal polymers as these are generally synthesized as macromolecules and require alignment post synthesis. Rather we focus on systems, like LC elastomers and physical gels that allow for alignment prior to solidification.

V. Polymerization of LCs

Polymers with liquid crystalline ordering are of significance to both the natural and man-made worlds. Both Kevlar and spider silk, two of the most remarkable polymeric materials from a mechanical standpoint, are processed in their liquid crystalline state.[56,57] Liquid crystal elastomers, first predicted by de Gennes[58] in 1975 and realized experimentally by Finkelmann and co-workers[59] in 1981, hold promise for energy dissipation, medical, and soft robotics applications. An advantage that liquid crystalline elastomers and polymer networks offer in the robotics application space is that they enable programming motion of millimeter[60,61] and micron-sized objects.[62,63] For instance, azobenzene containing liquid crystal elastomers have enabled light activated micro-walkers. These micro-walkers, made of liquid crystal elastomers and prepared using direct laser writing, are ~100 μm in size and can exhibit directed motion on laser irradiation.[63] Another advantage that liquid crystalline polymers offer is they can actuate underwater.[64,65] For instance, photo-responsive liquid crystal polymers have enabled the creation of artificial polyps that can grasp and release objects underwater.[66]

The traditional paradigm for liquid crystalline polymers has been to induce alignment after macromolecular synthesis. We discuss below solids produced through the alternate approach of polymerization of aligned small-molecule LCs. Assembly over larger volumes and access to a greater diversity of structures[67] are key advantages that polymerization post-alignment offers over alignment post-synthesis. We discuss below how these advantages have been leveraged to synthesize functional soft materials.

Organizing and polymerizing supramolecular LCs has been used to prepare polymer membranes where ion-conducting

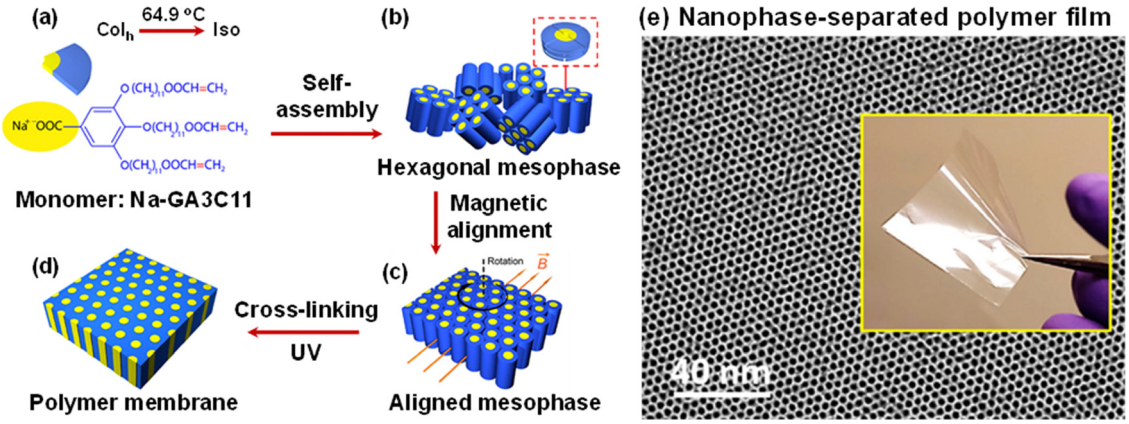

Fig. 5 Synthesis of polymer with oriented nanochannels through organization and curing of supramolecular LCs. (a) Molecular structure of supramolecular liquid crystal. (b) Assembly in the absence of magnetic field alignment. (c) Magnetic alignment of liquid crystal into homeotropic state. (d) Photopolymerization of aligned structure using ultraviolet radiation and (e) stained electron microscopy image showing uniform nanostructure. Inset in (e) shows a photographic image of the polymer being held with tweezers. Reproduced with permission from ref. 68. Copyright 2014 American Chemical Society.

nanochannels are anisotropically oriented over centimeter length-scales. In supramolecular LCs, the unit of assembly is a collection of molecules held together by weak interactions rather than a single molecule. An example of a supramolecular liquid crystal is shown in Fig. 5. The molecule consists of a sodium carboxylate core and photopolymerizable end groups. A few molecules self-assemble into a disk-shaped supramolecule. Osuji and co-workers aligned this supramolecular liquid crystalline system with a magnetic field of 6 Tesla. After assembly, the material was converted into a polymer through UV-curing. Shown in the inset of Fig. 5e is a photograph of the UV-cured polymer held with tweezers; the picture demonstrates the mechanical robustness of the material post-crosslinking. Transmission electron microscopy (TEM) is performed to image the nanostructure of the polymer. To generate contrast, ruthenium tetroxide (RuO_4), a staining agent which selectively binds to the benzene rings in the polymer is used. The TEM image in Fig. 5 reveals $\sim$1 nm large, hexagonally-packed dark spots. The dark spots correspond to the non-aromatic regions which form the nanochannels. The nanochannels in the aligned polymer are vertically aligned; the channel long-axis is parallel to the surface normal. The anisotropic organization of nanochannels facilitates ionic transport. The aligned membrane exhibits two orders of magnitude higher ionic conductivity relative to the polymer which was derived from the unorganized mesophase.

Aligned LCs and solids derived from them exhibit periodic nanoscale phase separation with pitches that are relevant for next-generation lithography. Solids derived from the polymerization of LCs, like the one shown in Fig. 5, hold promise for sub-5 nm patterning. However, for these polymers to be of practical interest for lithography, there needs to be a method to transfer these patterns into an inorganic substrate. In block-copolymer lithography, several approaches for pattern transfer exist including (1) the use of UV-radiation to erase one block and etching into exposed regions,[69,70] and (2) performing sequential infiltration synthesis[71–73] to incorporate metal oxides into the polar block and thereby increase etch contrast for subsequent plasma processing. It remains to be seen whether approaches like this are applicable to liquid crystalline systems. To the best of our knowledge, there are no successful reports of pattern transfer from a liquid crystalline solid to an inorganic substrate. Pattern transfer for liquid crystalline solids remains an important open problem. For an in-depth description of liquid crystal lithography and its potential, we direct the interested reader to a review on the subject by Nickmans and Schenning.[74]

Spatial patterning of molecular orientation in liquid crystalline solids can enable programming response to stimuli. Through patterning the anchoring conditions at the surface, complex liquid crystalline director fields can be achieved. The anchoring conditions can even be patterned such that liquid crystalline topological defects are created at precise locations in space. An example of this is shown in Fig. 6 where a 3×3 array of +1 topological defects is created through photopatterning of the underlying alignment layer. Complex director geometries, like the one shown in Fig. 6, are easily adopted in low molecular weight LCs. After LC assembly, the material is solidified. The chemistry of the precursor LC formulation is chosen such that the final solid is an elastomer. An elastomer is a lightly cross-linked and highly-stretchable polymer. As shown in Fig. 6b, when the elastomer with patterned molecular orientation is heated, the +1 defects respond through forming cones. Cone formation can enable actuation wherein the actuator lifts materials that are more than hundred times heavier than itself. Materials that exhibit programmed shape change and actuation in response to stimuli could be utilized for soft robotics. Like the polymer with aligned nanochannels discussed earlier, the conically actuating elastomer discussed here is realized through first imposing a specific molecular organization in the LC and then transferring that order to the solid state through polymerization.

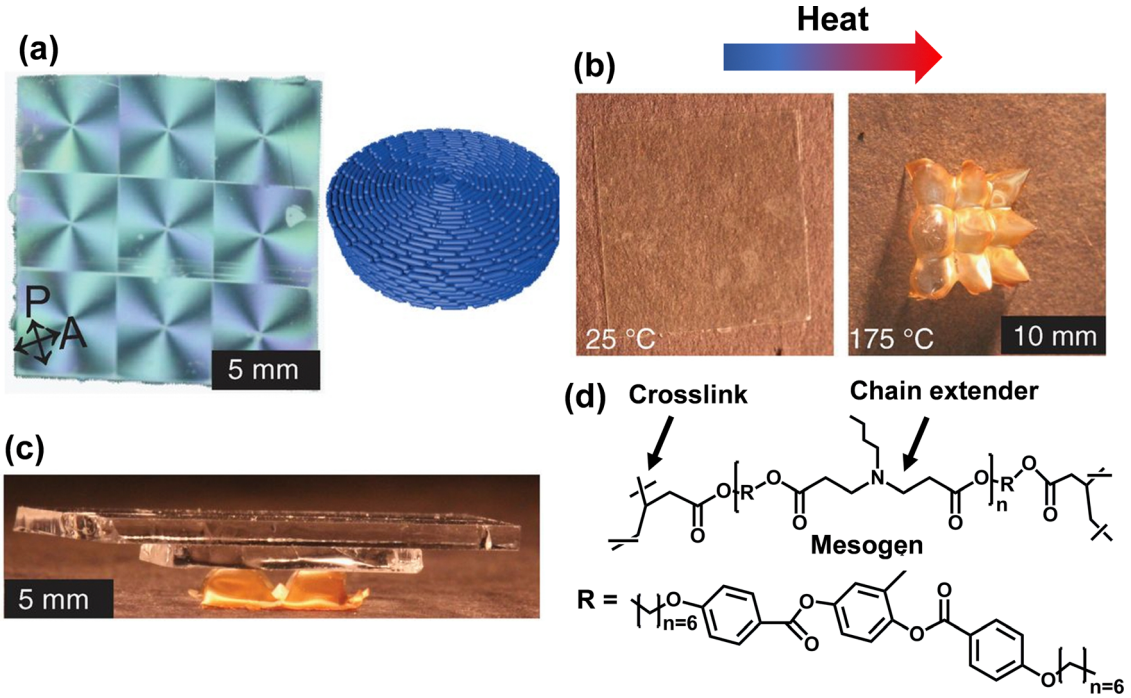

Fig. 6 Liquid crystal elastomers with programmed response to stimuli through defect engineering. (a) Array of +1 defects introduced into the LCs through controlling boundary condition. (b) Response to a liquid crystal elastomer with the patterned array to thermal response. Each +1 defect forms a conical structure upon heating into the isotropic phase. (c) Conical actuation using thermal stimuli. (d) Chemical structure of liquid crystal elastomer. The liquid crystal elastomer with programmed actuation was prepared through first imposing the organization shown in (a) in a small-molecule liquid crystal and then arresting that organization through photo-polymerization. Reproduced with permission from ref. 67. Copyright 2015 American Association for the Advancement of Science.

The traditional route of preparing aligned liquid crystal elastomers involves three steps. First, a partially cross-linked polymer is synthesized. After synthesis, the polymer is stretched and mechanically aligned. In the aligned state, the final cross-linking is performed. As discussed earlier, the elastomer in Fig. 6 was prepared using an alternate scheme. The desired director arrangement is achieved before polymerization of any kind is performed. This allows creating complex director patterns which in turn increase the complexity of programmable responses. The results in Fig. 6 provide an example of the benefits of alignment prior to solidification.

Introducing deformation modes into liquid crystal polymers can also be used to program response to stimuli. Through imposing different anchoring conditions at the top and bottom surface prior to polymerization, splay and twist deformations can be controllably introduced into the system. Subsequent polymerization results in a material that can respond to stimuli through bending and twisting.[75] Controlling liquid crystalline deformations such as splay, has formed the basis of soft robotic microgrippers. Weisrsma and co-workers created a microgripper with two pieces of light sensitive liquid crystalline polymer which were crossed together, and which had splayed molecular organization. When the material was exposed to light, owing to this splayed arrangement, the arms closed in a manner that enabled gripping.[62]

Responsive light crystalline polymers can be prepared through additive manufacturing (AM) techniques. Two-photon polymerization and direct ink-writing are examples of AM techniques that have been used to 3D-print liquid crystalline polymers.[75] Both techniques can be employed using an "organize and solidify" approach, wherein molecular organization is first imparted before polymerization.[75] In direct-ink writing, the shear forces in the printing nozzle can provide the orienting force, whereas in two-photon polymerization, a pulsed laser can be used to polymerize a pre-aligned liquid crystal photoresist. Additive manufacturing of liquid crystalline polymers has been used to produce soft robotic micro-walkers[63] and biomedical intervertebral implants.[76] The processing conditions in these applications, however, have not always been optimized for allowing alignment before polymerization. In the future, polymerizing pre-aligned nematics during AM could be used to enhance the performance of 3D printed liquid crystalline polymers.

The directed self-assembly and subsequent photopolymerization of LCs can be used to prepare solids with three-dimensional structures. Shown in Fig. 7 is a single polymeric photonic crystal formed from blue-phase liquid crystals (BPLCs). BPLCs occur in a narrow temperature window between the cholesteric and isotropic phases in chiral mixtures where the pitch <500 nm. As shown in Fig. 7, in blue-phase liquid crystals molecules organize into the double twist cylinders, which in turn organize into cubic lattices. The size of a BP lattice, which involves the assembly of millions of molecules, is $\sim$100 nm. Because their lattice sizes are comparable to the wavelength of visible light, blue-phases are photonic crystals.

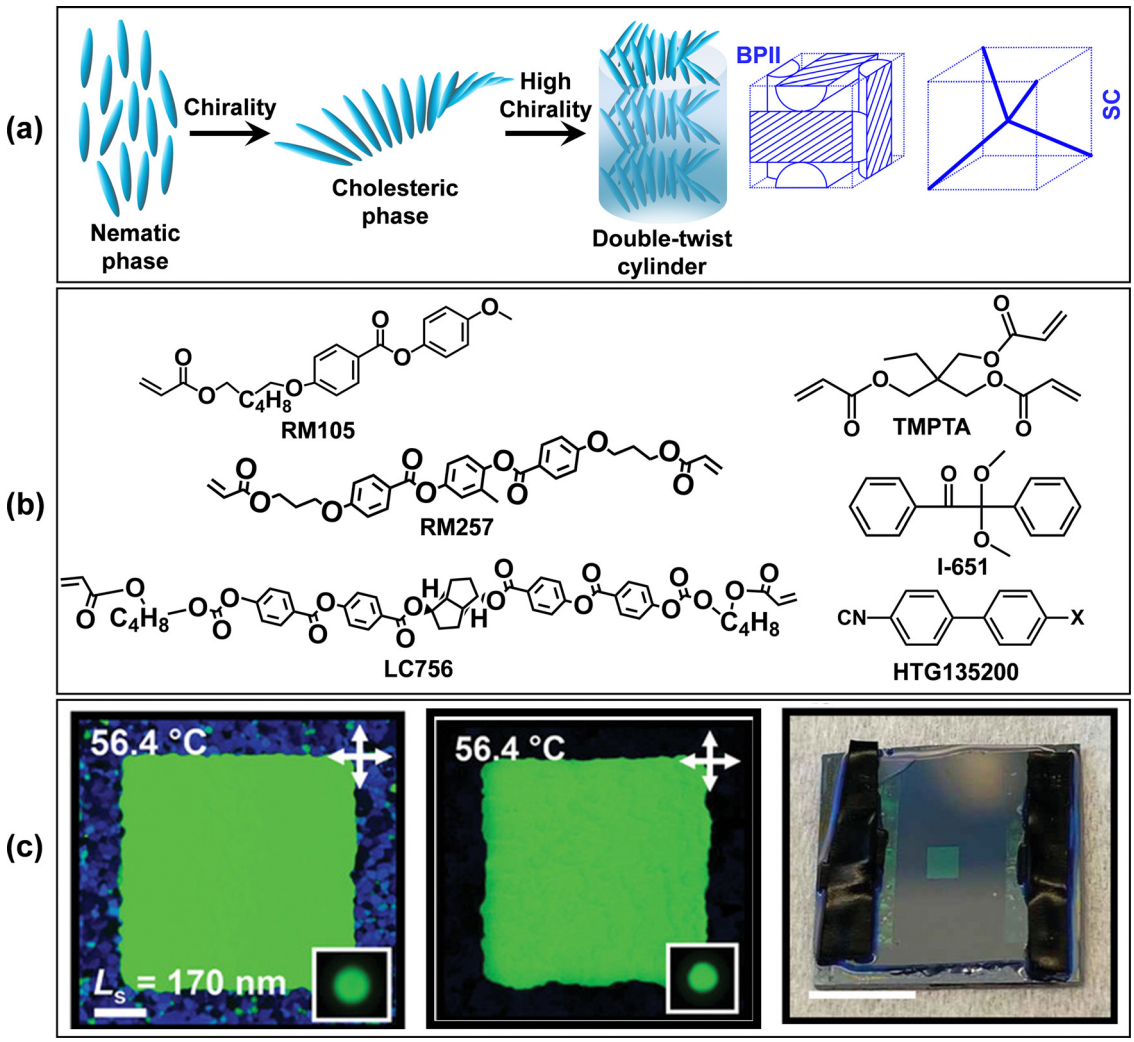

Fig. 7 Synthesis of polymeric, single photonic crystals from aligned blue phase liquid crystals. (a) Molecular organization in the simple cubic blue phase (BPII); molecules organize into double twist cylinders which in turn organize into a simple cubic lattice. Reproduced with permission from ref. 41. Copyright 2023 American Association for the Advancement of Science. (b) Molecular structure of components in a photopolymerizable blue phase. (c) Preparation of a polymeric single photonic crystal through the assembly and subsequent polymerization of blue phase liquid crystals. In (c), the image on the left is a polarized optical image of a ~500 μm long and wide square blue phase single crystal before polymerization while the image on the center shows a single crystal with the same dimensions after polymerization. The right most image in (c) is a photograph of a ~1 mm long and wide square blue phase single crystal surrounded by the un-patterned polycrystalline background. (b) and (c) are reproduced with permission from ref. 47 Copyright 2023 WILEY-VCH Verlag GmbH & Co. KGaA, Weinheim.

The color at which blue phases reflect light depends on their size (a), refractive index (n), and lattice orientation (specified by hkl). The reflection wavelength, λ, is given by the equation:

$$\lambda = \frac{2na}{\sqrt{(h^2 + k^2 + l^2)}} \quad (5)$$

For optical homogeneity, lattice alignment is essential and can be achieved either through rubbing polymeric substrates or through more sophisticated techniques like the use of chemical patterns. In Fig. 7, the square region contains a chemical pattern, whose pitch is equal to the lattice size, a condition that results in ⟨100⟩ lattice orientation. The region outside the patterned region is the un-patterned polycrystalline background. After alignment, the blue phase structure can be transferred to the polymeric state through UV radiation. The resulting solid is a polymeric single photonic crystal that is mechanically robust and thermally stable.[47]

Polymeric BPs respond to stimuli, like organic vapors, mechanical strain, or electric fields, through changing color, a feature that distinguishes them from inorganic photonic crystals. This property of polymeric BPs makes them promising for sensing applications. For instance, Abbott and co-worker demonstrated that polymerized blue-phases can sense toluene down to concentrations as low as 140 ppm.[77] Polymerized blue-phases have also been shown to produce easily observable optical changes to heptane, cyclohexane, dichloromethane, and ethanol vapors.[78] Yang and co-workers used polymerized blue phases to prepare humidity sensors whose color can be

used as reporters of RH from ten to eighty percent.[79] Polymerized blue phase gels and elastomers have also shown promising properties as mechanochromic strain sensors.[17,38] For an in-depth review of the properties and applications of BP based polymers, we direct the reader to a recent review.[41]

In this section, we focused our discussion on the synthesis and applications of responsive materials through the polymerization of small-molecule LCs. Liquid crystalline gels and elastomers are the most responsive material classes in the group of liquid-crystal derived polymeric solids.

Nanoparticles are often added to liquid crystalline polymers to render new functionality to them. Nanoparticles that have been added to liquid crystalline polymers include carbon nanotubes,[80] magnetic nanoparticles,[81] and quantum dots.[82] Carbon nanotubes incorporated into liquid crystalline polymers have shown promise for dynamic Braille displays. The photo-actuating properties of these composite materials can be used to reversibly switch surface topography.[83] The incorporation of nanoparticles is compatible with the align and solidify approach for synthesis of solids with liquid crystalline order, the overarching focus of the present article. White and co-workers were able to simultaneously organize the small-molecule LC precursor and the carbon nanotube additive into a concentric director field like the one shown in Fig. 6. This organization was then transferred to the solid state through photopolymerization. Carbon nanotube addition to liquid elastomers enabled electrically driven shape transformation in this case. Shape changes in neat liquid crystal elastomers are usually driven by light or temperature.

VI. Physical gelation in LCs

Gelation is the process whereby the solute forms a large network in the solvent, resulting in the response of the solution changing from liquid-like to solid-like. Gels can be either chemical or physical. In chemical gels, the units comprising the network are held together by covalent bonds. Gels of this kind can be formed by photo-polymerization of the solutes and have been discussed in the previous section. For instance, the blue-phase formulation shown in Fig. 7 forms a chemical gel upon UV-curing. In this section we discuss physical gels, where the units comprising the network are held together by weak non-covalent interactions like hydrogen bonding. When physical gelation occurs after a liquid crystal transition, macroscopically organized, soft solids can be formed.

Liquid crystal physical gels contain a mixture of a mesogen and low-molecular weight organic gelator (LMOG). Below the sol–gel transition temperature, the gelator forms a large network held together by supramolecular interactions. Most organic gelators, like the ones shown in Fig. 8, form networks through hydrogen-bonding. The sol–gel transition temperature can be either higher or lower than the isotropic-liquid crystal transition temperature. As shown in Fig. 8, during cooling when gelation occurs before mesophase formation, an unaligned mesh-like network is formed. However, when the liquid crystal phase forms first and is aligned later, gelation results in formation of long, needle-like fibers. In this scenario, both molecular and fiber orientation in the gel can be controlled. An atomic force microscope (AFM) image of an aligned fiber in a liquid crystal physical gel is shown in Fig. 8.

Liquid crystal physical gels show promising properties for electro-optic applications.[85–87] In liquid crystal display (LCD) devices, oriented nematic physical gels exhibit faster response times and lower threshold voltages than the pure nematic without the gelator.[88] In addition to traditional twisted cell-LCDs, liquid crystal physical gels have also shown promise for bistable electro-optic devices. In these devices, stable transparent and light-scattered states are formed using nematic physical gels. The transparent state is created through cooling in the presence of an electric field. Homeotropic alignment is retained after removal of the field because of gelation which occurs at a lower temperature than the isotropic to nematic transition. Heating into the isotropic states resets the system and cooling in the absence of an electric field leads to an unaligned nematic gel which scatters light and is therefore turbid. LCs physical gels therefore provide access to stable transparent and turbid states at the same temperature and for the same composition.

Physical gelation has been used to prepare solid and responsive photonic crystals from blue-phase liquids crystals.[89] Nair

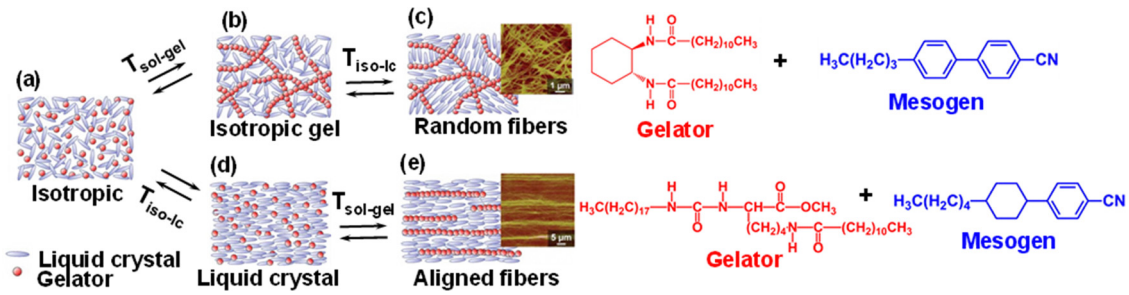

Fig. 8 Gelation in blends of liquid crystal formers and low-molecular weight organic gelator (LMOG). (a) Structure in the isotropic phase. (b) Gelation in the isotropic phase and (c) liquid crystal phase formed in an isotropic gel. AFM image shows the randomly oriented gel fibers that form through this route. (d) Liquid crystal phase structure before gelation and (e) liquid crystal physical gel after gelation in an oriented solvent. AFM image shows ordered gel fibers that form through this later route. The red and blue molecules shown on the right are the gelator and mesogen molecules, respectively. Reproduced with permission from ref. 84. Copyright 2007 The Royal Society of Chemistry.

and co-workers mixed LMOG 12-hydroxystearic acid, into a blue-phase formulation. In the studied mixture, the sol–gel transition temperature occurs below the BP transition. The blue phase physical gel, studied by Nair and co-workers, exhibits reversible color changes in response to electric fields, a property that could be used for camouflage applications. The change in color was driven by different lattice orientations adopted in the presence and absence of electric fields.

VII. Vitrification of LCs

In addition to polymerization and physical gelation, liquid crystalline ordering can be transferred to the solid state through glass formation. Glasses derived from quenching LCs or "glassy LCs" as we shall subsequently refer to them combine the structural anisotropy of LCs with the slow dynamics of amorphous solids. The moduli of glassy LCs are in 1–10 GPa range as shown in Fig. 4.

The transformation of a glassy liquid crystal upon heating, as observed in the laboratory, is a kinetic process, unlike the melting of a crystalline solid, which is a true thermodynamic phase transition. At the glass transition temperature T_g, there are no discontinuities in either the first or second derivatives of free energy. As a material is heated above T_g, the only event that occurs is that the timescales for molecular motions go from becoming too long to measure in the glass state to being observable in the supercooled liquid. Like conventional isotropic glasses, glassy LCs transform into the more mobile supercooled liquid phase *via* a glass transition. Despite their anisotropic structure, it is the nature of their transition from or to the supercooled liquid phase, that justifies classifying glassy LCs as glasses. Below we briefly introduce the molecular systems that can be vitrified into glassy LCs and then discuss the potential these materials hold for applications.

Canonical mesogens exhibit liquid crystalline phases between the clearing and crystallization temperatures. Textbook liquid crystal formers 5CB and 8CB fall into this class of molecules. For a rarer class of mesogens, however, the liquid crystalline phases occur below the freezing point. Examples of mesogens that exhibit LC phases in the supercooled liquid regime include antifungal drug molecule Itraconazole and organic semiconductor phenanthroperylene-ester (Fig. 9). These supercooled LCs form glassy solids when cooled to sufficiently low temperatures and at rates fast enough to avoid crystallization.

One of the defining characteristics of glassy solids is that their properties depend on thermal history. A common process parameter used to tune both the enthalpy and density of amorphous solids is the cooling rate used for glass formation from the precursor liquid state. Glasses prepared through a slower cooling rate are lower in enthalpy and more dense owing to the larger time provided for equilibration. While glassy LCs are also expected to exhibit this behavior, the cooling rate also influences the degree of structural order in these materials. Shown in Fig. 9 are illustrations of packing in glasses of phenanthroperylene-ester prepared using different cooling rates. The material prepared using fast cooling rate exhibits the disorder typically associated with nematic glasses, while a slow cooling rate yields a highly structured solid. Different electronic applications might require different levels of order. For efficient transport, highly anisotropic structure is desired. A less ordered and tightly packed structure, however, might be able to incorporate a higher percentage of dopants, which are commonly introduced in organic semiconductors to render luminescence or electronic conductivity. The structure of glassy LCs can be tailored for the specific application of interest.

The primary advantages glassy LCs offer is their facile structural and compositional tunability. As discussed above, for glass-forming LCs, a library of solids, with continuously

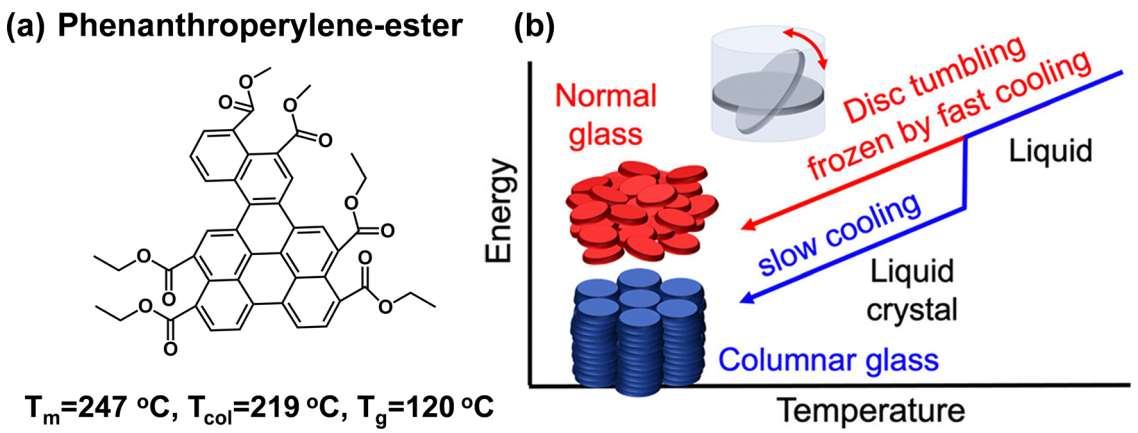

Fig. 9 Anisotropic solid formation through vitrification of LCs. (a) Molecular structure of phenanthroperylene-ester, a molecule that exhibits a columnar phase at a temperature (T_{col}) below the melting point (T_m) and which forms solids with liquid crystalline order when cooled below the glass transition temperature, T_g. Molecules that form liquid crystalline phases below the melting points and which can be quenched into a glassy solid are rare. (b) Cooling rate dependent structure in liquid crystalline glasses of phenanthroperylene-ester. Fast cooling produces high energy glasses that exhibit only nematic order while slow cooling produces low energy glasses that exhibit columnar hexagonal order. Reproduced with permission from ref. 90. Copyright 2021 American Chemical Society.

varying degrees of order can be prepared by changing the cooling rate. For crystals, in contrast, the number of different structures is limited by the number of possible polymorphs. Some molecules, like 9,10-anthraquinone, are known to exhibit only a single crystal structure.[91] Even amongst the compounds that exhibit polymorphism, ≈90% exhibit only two different crystal structures.[91] Forming glassy solids through rapidly cooling LCs therefore provides greater tunability than traditional crystal growth. As LCs are compositionally flexible, the same is also true for solids derived from quenching them.

The properties of glassy LCs make them promising for photonic applications.[92] Of particular interest are glasses of cholesteric or chiral nematic LCs which have been used to produce circularly polarized light through luminescence. Owing to their periodic helical structure, cholesterics exhibit Bragg's reflection of light. The wavelength of reflection, λ, is highly tunable. As explained earlier, cholesteric LCs contain a mixture of chiral dopant and an achiral nematic liquid crystal. The concentration of the chiral dopant (c) and its helical twisting power (HTP) determine the pitch (p). The pitch in turn determines the wavelength of reflected light (λ). The relationship between these quantities is given mathematically by:

$$p = \frac{1}{\mathrm{HTP} \times C} \tag{6}$$

$$\lambda = np\cos\phi \tag{7}$$

where n is the refractive index and ϕ is the angle between the cholesteric helix and the incoming radiation. Through doping a luminophore in a chiral nematic glass, Chen *et al.* achieved nearly pure circularly polarized luminescence.[93] Achieving high degrees of circularly polarized luminescence is desirable for applications such as 3D displays. Here the tunable structure and composition of glassy LCs, discussed earlier, play an important role. To produce polarized luminescence, Chen *et al.* tuned the composition such that the reflection spectrum of chiral nematic host overlapped with the luminescence spectrum of the emissive molecule.

Thin films of glassy LCs can be produced through physical vapor deposition (PVD). In PVD, the material of interest is either evaporated or sublimed in a high vacuum chamber. Gaseous molecules then condense onto a substrate to form solid films. When glass-forming mesogens are deposited through PVD, they provide exquisite control over molecular orientation. Both columnar order in discotic mesogens and smectic order in calamitic mesogens can be continuously tuned; either through varying the deposition temperature or rate. For PVD film of Itraconazole; by choosing different deposition conditions, any average tilt angle for the molecular long axis between 27 and 76 degrees could be selected.[94]

Glassy LCs prepared through PVD exhibit promising properties for organic electronic applications.[95] For phenathoperelyene ester, by tuning the deposition conditions, either face-on or edge-on packing can be attained.[96,97] Face-on packing and edge-in packing are desirable for different device geometries. Edge-on packing is desirable for devices such as OFETs which require efficient in-plane charge transport, where face-on packing can promote efficient out-of-plane electric conduction, which is beneficial for devices such as OLEDs. Irrespective of whether glassy LCs are prepared through liquid cooling or PVD, their structure can be continuously tuned through varying processing conditions.

A remarkable feature of PVD is that it can be used to produce glasses with nematic-like[14,98,99] and smectic-like[100] order from molecules that do not exhibit liquid crystalline phases. The surface-equilibration mechanism provides an explanation for the bulk anisotropic structure in PVD glasses.[100–102] The basis of the mechanism is the enhanced mobility at the surface of molecular glasses; the surface of molecular glasses can be seven orders of magnitude more mobile than the bulk.[103] As PVD is a layer-by-layer process, all molecules at some point are at the mobile free surface. During their time at the vacuum interphase of the growing films, molecules naturally adopt configurations favored at the surface of the liquid. When buried by subsequent depositions, these surface-favored configurations get trapped into the bulk.[100] Unlike the bulk of liquids and traditional glasses which are isotropic, the surface can exhibit anisotropic structure. PVD therefore also creates structure through the "organize and solidify" approach. Order is created when the molecules are part of the mobile surface layer, and solidification occurs after structure has been created.

VIII. Conclusions and future problems

In earlier sections, we discussed the use of small-molecule liquid crystal precursors for the macroscopic control of nanostructure in organic solids. Before discussing future opportunities and challenges, we summarize the advantages of this approach over both traditional crystallography and the directed self-assembly of other soft materials.

The primary advantages of forming solids from small-molecule, thermotropic LCs over using traditional crystallography are:

(1) Solidification of LCs is often a more scalable approach than crystal growth which can be limited by slow kinetics for molecular systems.

(2) Liquid crystalline elastomers and gels are responsive and stretchable, and in this sense exhibit better mechanical properties than molecular crystals which tend to be non-responsive and brittle.

(3) Like their fluid precursors, liquid crystalline solids exhibit structural flexibility. In a liquid crystalline solid, the average tilt angle with respect to the surface normal can be continuously tuned.[104] Moreover, molecular orientation can be spatially patterned, a feature that allows for programmed response to stimuli. We are unaware of examples of programming material response to stimuli using molecular crystals.

Directed self-assembly (DSA) is a bottom-up approach to control the microstructure of materials. A variety of self-assembling soft materials are used in DSA such as LCs, block co-polymers[105–108] and colloids.[109] Block-copolymers are used for many of the same applications discussed in this review like

the fabrication of photonic crystals[110] or iso-porous membranes.[111] LCs and solids derived from them offer the following advantages over block-copolymers for the macroscopic control of nanostructure:

(1) LCs can uniformly assemble over larger areas than block co-polymers. For instance, both discotic LCs and block-copolymers self-organize in microchannels through a process referred to as grapho-epitaxy. Whereas discotic LCs exhibit directional planar anchoring in channels as wide as 25 μm, uniform domain orientation in block co-polymers usually requires channels that are hundred times narrower.[51,112]

(2) LCs offer facile access to small length-scale features. Accessing small feature sizes in soft materials is of interest for both membrane technology and lithography. The unit of assembly in LCs is a molecule, and feature sizes like the ones shown in Fig. 5 can have molecular dimensions. These liquid crystalline systems exhibit feature sizes of ~1 nm. In the cylindrical phase of PS-PMMA, the fruit-fly system of block co-polymer lithography, the smallest accessible feature size is ~10 nm. Access to smaller feature sizes using block co-polymers is only possible in systems with such low molecular weight that they could effectively be regarded as small-molecules. The oligomeric block co-polymers that give access to the smallest feature sizes are essentially LCs.[113]

Despite the advances in the assembly of liquid crystalline solids from small molecule liquid precursors, several challenges, unanswered questions, and research opportunities exist in this area. A practical challenge is that many of the alignment methods like nanopatterned surface or magnetic field-directed self-assembly are complex and expensive methods. The material in Fig. 5 was produced using a magnetic field of 6 T. This field strength is higher than that produced by most clinical MRI (magnetic resonance imaging) magnets. The polymeric single photonic crystal in Fig. 7 was formed through assembling the precursor small molecule liquid crystal phase using electron beam lithography, a technique that is both expensive and exhibits limited scalability. There is a need for facile and large area assembly methods for producing liquid crystalline solids through the align and solidify approach discussed in this review. The production of nanostructured surfaces for liquid crystal assembly using interference lithography is a promising approach. The technique is highly applicable for patterning large surfaces. Recently, 1 cm^2 blue phase single crystals were prepared using the technique.[114] Advances in large area patterning could be leveraged to access even larger assembly volumes in the future.

Some important and under-explored areas of research pertaining to liquid crystalline solids are:

(1) **Understanding liquid crystal–polymer nanocomposites:** Polymer composites are an important material class that are of interest for diverse sectors ranging from the automotive tire industry to spacecraft construction.[115–117] One of the major problems in the field of polymer nanocomposites is controlling the dispersion of nanoparticles.[118] Topological defects in LCs are known to trap nanoparticles.[119,120] As discussed earlier in the review, topological defects in LCs can be controllably introduced into the system through controlling the surface anchoring conditions. In some liquid crystalline phases, like the blue phase (Fig. 7), an ordered lattice of topological defects exists at equilibrium. Nanoparticle lattices can therefore be formed in small-molecule LCs, like blue phases, by using topological defects to trap particles. Polymerization after the assembly of nanoparticles in the LCs leads to a nanocomposite. Polymerization of LCs where nanoparticles are localized at the defects could provide one route to control dispersion in polymer nanocomposites. Systematic studies of polymer nanocomposites derived from polymerization of small-molecule LCs are required to determine whether materials derived from this route can meet specific application needs and offer advantages over more traditional routes of preparing polymer nanocomposites. We note that while liquid crystalline polymer nanocomposites have been investigated,[80–82] and some materials in this class have already demonstrated promise for applications, the methods used to produce them have not leveraged the ability of topological defects to trap nanoparticles. It is production of polymer nanocomposites through this route, and the evaluation of their properties, that we believe warrants more exploration. Liquid crystal polymer nanocomposites prepared through more traditional routes also seem to suffer from a lack of nanoparticle dispersion.[81]

Liquid crystal gels are also composite materials. This is apparent in the AFM image shown in Fig. 8 where micro-scale fibers in a liquid crystalline matrix can be seen. While the electrooptical properties of liquid crystal gels have been extensively studied, especially in the context of LCD devices, other aspects of their behavior remain largely unexplored. A better understanding of the transport, mechanics, and rheology of these materials could help us identify applications where replacing isotropic gels with their anisotropic counterparts would be advantageous. Isotropic gels are being widely explored for healthcare and energy applications.

(2) **Understanding and predicting aging of liquid crystalline solids:** Glasses are out-of-equilibrium materials and their properties therefore gradually change over time though a process called physical aging. As long-term material stability is an important consideration for almost any application, and as glasses are broadly utilized in technology, physical aging has been studied extensively. For isotropic glasses, a variety of first-principles[121,122] and phenomenological models[123] have been developed to understand and predict aging. An important unanswered question is whether these aging models are applicable for the molecular and polymeric glasses with liquid crystalline order that we have discussed in this review. Experiments aimed at answering this question are essential for developing an understanding of the stability of molecular and polymeric glasses with liquid crystalline order, which in turn is key for using these materials in applications. Gels can also exhibit physical aging.[124] Understanding whether liquid crystalline ordering influences the aging of gels is essential if these materials are to be used for applications.

Preliminary studies show that glassy liquid crystals can take longer times to return to an equilibrium state than their

isotropic counterparts.[96] A possible reason for this could be that equilibration involves the concerted motion of a larger number of molecules in liquid crystal systems. Provided the results for glass rejuvenation above T_g are applicable to aging, imparting liquid crystalline ordering to non-equilibrium solids could be a strategy to slow aging and increase stability.

(3) **Rational design and accelerated discovery of liquid crystalline solids:** Artificial intelligence is playing an important role in advancing the molecular sciences, from protein structure prediction[125] to autonomous laboratories for rapid sampling of material processing parameter spaces.[126–128] Artificial intelligence is likewise being extensively applied to liquid crystal science.[129,130] Molecular descriptor based neural networks have been trained to predict clearing temperatures for traditional calamatic[131] as well as bent-core liquid crystals[132] while random forest models have been developed that predict the existence of liquid crystalline phases from molecular structure.[133]

The rapid advances in artificial intelligence could be leveraged to advance the field of liquid crystalline solids as well. We discussed earlier preparing anisotropic organic solids through the vitrification of small-molecule liquid crystals, a process that requires identifying molecules that are simultaneously good glass-formers and exhibit liquid crystalline phases. Till date the co-existence of these attributes has been found for only a handful of molecules. Advanced machine learning approaches could be used to generate a large library of molecules that are likely to be glass-forming liquid crystals even before they are synthesized. Such efforts could be based on using as training data the large libraries of known small-molecule glass-formers and liquid crystal formers, as well as the relatively small library of known glass-forming liquid crystals. A machine learning-guided, rational design approach would dramatically increase the number, range, and functionality of glassy liquid crystals.

The preparation of liquid crystalline polymers and physical gels from the assembly and solidification of small-molecules could similarly benefit from AI. Liquid crystal gels and polymers are formed from the solidification of multicomponent small-molecule mixtures. Photopolymerizable small molecule mixtures, like the one shown in Fig. 7, contain photo-initiators, cross-linkers, reactive mesogens, and non-polymerizable small-molecule mesogens. Determination of compositions that exhibit the desired phase behavior occurs through a combination of intuition-based and trial-and-error approaches. Machine learning could allow for rational design of liquid crystalline polymers and gels through enabling predictive ability of the phase behavior of precursor liquid formulations. Ideally, such predictions of phase behavior would be based on molecular structures and composition alone and the predicted variables would include the type and temperature ranges of liquid crystal phases.

Data availability

No primary research results, software or code have been included and no new data were generated or analyzed as part of this review entitled ''Liquid crystals as Solid-State Templates''.

Conflicts of interest

There are no conflicts to declare.

Acknowledgements

We acknowledge startup funds provided by Rice University

References

1 G. Sun, J. Xu and P. Harrowell, *Nat. Mater.*, 2018, **17**, 881–886.
2 D. M. Herlach, D. Simons and P.-Y. Pichon, *Philos. Trans. R. Soc., A*, 2018, **376**, 20170205.
3 D. Musumeci, M. Hasebe and L. Yu, *Cryst. Growth Des.*, 2016, **16**, 2931–2936.
4 S. Z. D. Cheng, J. Chen and J. J. Janimak, *Polymer*, 1990, **31**, 1018–1024.
5 R. K. Bowles and P. Harrowell, *J. Phys. Chem. B*, 2023, **127**, 4126–4134.
6 T. Kato, M. Yoshio, T. Ichikawa, B. Soberats, H. Ohno and M. Funahashi, *Nat. Rev. Mater.*, 2017, **2**, 1–20.
7 Y. Cang, Z. Wang, C. Bishop, L. Yu, M. D. Ediger and G. Fytas, *Adv. Funct. Mater.*, 2020, **30**, 2001481.
8 M. T. Cicerone and J. F. Douglas, *Soft Matter*, 2012, **8**, 2983–2991.
9 L. Yu, *Adv. Drug Delivery Rev.*, 2001, **48**, 27–42.
10 S. Zhang, F. Talnack, T. Jousselin-Oba, V. Bhat, Y. Wu, Y. Lei, Y. Tomo, H. Gong, L. Michalek and D. Zhong, *et al.*, *J. Mater. Chem. C*, 2023, **11**, 8992–9001.
11 M. Sawatzki-Park, S.-J. Wang, H. Kleemann and K. Leo, *Chem. Rev.*, 2023, **123**, 8232–8250.
12 J. Song, H. Lee, E. G. Jeong, K. C. Choi and S. Yoo, *Adv. Mater.*, 2020, **32**, 1907539.
13 D. Yokoyama, *J. Mater. Chem.*, 2011, **21**, 19187–19202.
14 K. Bagchi and M. D. Ediger, *J. Phys. Chem. Lett.*, 2020, **11**, 6935–6945.
15 Y. Shirota, *J. Mater. Chem.*, 2005, **15**, 75–93.
16 C. W. Tang and S. A. VanSlyke, *Appl. Phys. Lett.*, 1987, **51**, 913–915.
17 F. Castles, S. M. Morris, J. M. C. Hung, M. M. Qasim, A. D. Wright, S. Nosheen, S. S. Choi, B. I. Outram, S. J. Elston and C. Burgess, *et al.*, *Nat. Mater.*, 2014, **13**, 817–821.
18 K. M. Herbert, H. E. Fowler, J. M. McCracken, K. R. Schlafmann, J. A. Koch and T. J. White, *Nat. Rev. Mater.*, 2022, **7**, 23–38.
19 M. Barnes and R. Verduzco, *Soft Matter*, 2019, **15**, 870–879.
20 L. Li, J. Walda, L. Manna and A. P. Alivisatos, *Nano Lett.*, 2002, **2**, 557–560.
21 S. Zhang and S. Kumar, *Small*, 2008, **4**, 1270–1283.
22 A. D. Rey, *Soft Matter*, 2010, **6**, 3402–3429.
23 Q. Mu, Z. Cao, L. Hu, D. Li and L. Xuan, *Opt. Express*, 2006, **14**, 8013–8018.
24 Y. Yang, A. Forbes and L. Cao, *Opto-Electron. Sci.*, 2023, **2**, 230021–230026.

25 I.-H. Lin, D. S. Miller, P. J. Bertics, C. J. Murphy, J. J. de Pablo and N. L. Abbott, *Science*, 2011, **332**, 1297–1300.
26 S. E. Robinson, B. A. Grinwald, L. L. Bremer, K. A. Kupcho, B. R. Acharya and P. D. Owens, *J. Occup. Environ. Hyg.*, 2014, **11**, 741–750.
27 S. Yang, C. Wu, H. Tan, Y. Wu, S. Liao, Z. Wu, G. Shen and R. Yu, *Anal. Chem.*, 2013, **85**, 14–18.
28 S. Urban, B. Gestblom, W. Kuczyński, S. Pawlus and A. Würflinger, *Phys. Chem. Chem. Phys.*, 2003, **5**, 924–928.
29 J. Jiang, D. M. Walters, D. Zhou and M. D. Ediger, *Soft Matter*, 2016, **12**, 3265–3270.
30 D. M. Walters, L. Antony, J. J. de Pablo and M. D. Ediger, *J. Phys. Chem. Lett.*, 2017, **8**, 3380–3386.
31 K. Tanaka, *J. Chem. Soc., Faraday Trans. 1*, 1975, **71**, 1127–1131.
32 S. V. Dvinskikh, I. Furó, H. Zimmermann and A. Maliniak, *Phys. Rev. E: Stat., Nonlinear, Soft Matter Phys.*, 2002, **65**, 61701.
33 S. V. Dvinskikh, I. Furó, H. Zimmermann and A. Maliniak, *Phys. Rev. E: Stat., Nonlinear, Soft Matter Phys.*, 2002, **65**, 50702.
34 L. Zhu, C. W. Brian, S. F. Swallen, P. T. Straus, M. D. Ediger and L. Yu, *Phys. Rev. Lett.*, 2011, **106**, 256103.
35 S. Meiboom, J. P. Sethna, P. W. Anderson and W. F. Brinkman, *Phys. Rev. Lett.*, 1981, **46**, 1216.
36 C.-W. Chen, C.-T. Hou, C.-C. Li, H.-C. Jau, C.-T. Wang, C.-L. Hong, D.-Y. Guo, C.-Y. Wang, S.-P. Chiang and T. J. Bunning, *et al.*, *Nat. Commun.*, 2017, **8**, 1–8.
37 W. Hu, L. Wang, M. Wang, T. Zhong, Q. Wang, L. Zhang, F. Chen, K. Li, Z. Miao and D. Yang, *et al.*, *Nat. Commun.*, 2021, **12**, 1–8.
38 K. R. Schlafmann and T. J. White, *Nat. Commun.*, 2021, **12**, 4916.
39 H. Kikuchi, M. Yokota, Y. Hisakado, H. Yang and T. Kajiyama, *Nat. Mater.*, 2002, **1**, 64–68.
40 J. A. Martinez-González, X. Li, M. Sadati, Y. Zhou, R. Zhang, P. F. Nealey and J. J. de Pablo, *Nat. Commun.*, 2017, **8**, 1–9.
41 K. Bagchi, T. Emeršič, J. A. Martinez-González, J. J. de Pablo and P. F. Nealey, *Sci. Adv.*, 2023, **9**, eadh9393.
42 I. Dierking, *Symmetry*, 2014, **6**, 444–472.
43 C. F. Dietrich, P. J. Collings, T. Sottmann, P. Rudquist and F. Giesselmann, *Proc. Natl. Acad. Sci. U. S. A.*, 2020, **117**, 27238–27244.
44 Q. Zhang, W. Wang, S. Zhou, R. Zhang and I. Bischofberger, *Nat. Commun.*, 2024, **15**, 7.
45 P.-G. De Gennes and J. Prost, *The physics of liquid crystals*, Oxford University Press, 1993.
46 Y. H. Kim, D. K. Yoon, H. S. Jeong, O. D. Lavrentovich and H.-T. Jung, *Adv. Funct. Mater.*, 2011, **21**, 610–627.
47 T. Emeršič, K. Bagchi, J. A. Martinez-González, X. Li, J. J. de Pablo and P. F. Nealey, *Adv. Funct. Mater.*, 2022, 2202721.
48 D. W. Berreman, *Mol. Cryst. Liq. Cryst.*, 1973, **23**, 215–231.
49 J. J. Skaife and N. L. Abbott, *Chem. Mater.*, 1999, **11**, 612–623.
50 M. F. Toney, T. P. Russell, J. A. Logan, H. Kikuchi, J. M. Sands and S. K. Kumar, *Nature*, 1995, **374**, 709–711.
51 J. Cattle, P. Bao, J. P. Bramble, R. J. Bushby, S. D. Evans, J. E. Lydon and D. J. Tate, *Adv. Funct. Mater.*, 2013, **23**, 5997–6006.
52 K. Bagchi, T. Emersic, Z. Wang, W. Chen, M. Kim, C. Eom, Z. Jiang, J. Strzalka, J. J. de Pablo and P. F. Nealey, *J. Mater. Chem. C*, 2023, **11**, 11466–11475.
53 Y. Guo, H. Shahsavan, Z. S. Davidson and M. Sitti, *ACS Appl. Mater. Interfaces*, 2019, **11**, 36110–36117.
54 Y. Zhao, J. Li, Y. Yu, Y. Zhao, Z. Guo, R. Yao, J. Gao, Y. Zhang and D. Wang, *Molecules*, 2022, **27**, 7265.
55 P. Salamon, Z. Karaszi, V. Kenderesi, Á. Buka and A. Jákli, *Phys. Rev. Res.*, 2020, **2**, 23261.
56 D. Tanner, J. A. Fitzgerald and B. R. Phillips, *Angew. Chemie*, 1989, **101**, 665–670.
57 D. P. Knight and F. Vollrath, *Philos. Trans. R. Soc., B*, 1999, **266**, 519–523.
58 P. G. De Gennes, *CR Acad. Sci. Ser., B*, 1975, **281**, 101–103.
59 H. Finkelmann, H.-J. Kock and G. Rehage, *Die Makromol. Chemie, Rapid Commun.*, 1981, **2**, 317–322.
60 O. M. Wani, H. Zeng and A. Priimagi, *Nat. Commun.*, 2017, **8**, 15546.
61 M. da Cunha, S. Ambergen, M. G. Debije, E. F. G. A. Homburg, J. M. J. den Toonder and A. P. H. J. Schenning, *Adv. Sci.*, 2020, **7**, 1902842.
62 D. Martella, S. Nocentini, D. Nuzhdin, C. Parmeggiani and D. S. Wiersma, *Adv. Mater.*, 2017, **29**, 1704047.
63 H. Zeng, P. Wasylczyk, C. Parmeggiani, D. Martella, M. Burresi and D. S. Wiersma, *Adv. Mater.*, 2015, **27**, 3883.
64 W. Seo, C. S. Haines, H. Kim, C.-L. Park, S. H. Kim, S. Park, D.-G. Kim, J. Choi, R. H. Baughman and T. H. Ware, *et al.*, *Small*, 2024, 2406493.
65 Y. Nemati, Q. Yang, F. Sohrabi, J. V. I. Timonen, C. Sánchez-Somolinos, M. Honkanen, H. Zeng and A. Priimagi, *ACS Appl. Mater. Interfaces*, 2025, **17**, 5316–5325.
66 M. da Cunha, H. S. Kandail, J. M. J. den Toonder and A. P. H. J. Schenning, *Proc. Natl. Acad. Sci. U. S. A.*, 2020, **117**, 17571–17577.
67 T. H. Ware, M. E. McConney, J. J. Wie, V. P. Tondiglia and T. J. White, *Science*, 2015, **347**, 982–984.
68 X. Feng, M. E. Tousley, M. G. Cowan, B. R. Wiesenauer, S. Nejati, Y. Choo, R. D. Noble, M. Elimelech, D. L. Gin and C. O. Osuji, *ACS Nano*, 2014, **8**, 11977–11986.
69 F. Ferrarese Lupi, T. J. Giammaria, F. G. Volpe, F. Lotto, G. Seguini, B. Pivac, M. Laus and M. Perego, *ACS Appl. Mater. Interfaces*, 2014, **6**, 21389–21396.
70 G. Freychet, M. Maret, R. Tiron, X. Chevalier, A. Gharbi, M. Fernandez-Regulez and P. Gergaud, *J. Polym. Sci., Part B: Polym. Phys.*, 2016, **54**, 1137–1144.
71 Q. Peng, Y.-C. Tseng, S. B. Darling and J. W. Elam, *ACS Nano*, 2011, **5**, 4600–4606.
72 R. Z. Waldman, D. Choudhury, D. J. Mandia, J. W. Elam, P. F. Nealey, A. B. F. Martinson and S. B. Darling, *JOM*, 2019, **71**, 212–223.
73 C. Liu, K. Yoshimoto, J. de Pablo and P. Nealey, *Microlithography*, CRC Press, 2020, pp. 767–824.

74 K. Nickmans and A. P. H. J. Schenning, *Adv. Mater.*, 2018, **30**, 1703713.
75 M. Del Pozo, J. A. H. P. Sol, A. P. H. J. Schenning and M. G. Debije, *Adv. Mater.*, 2022, **34**, 2104390.
76 R. H. Volpe, D. Mistry, V. V. Patel, R. R. Patel and C. M. Yakacki, *Adv. Healthcare Mater.*, 2020, **9**, 1901136.
77 Y. Yang, Y.-K. Kim, X. Wang, M. Tsuei and N. L. Abbott, *ACS Appl. Mater. Interfaces*, 2020, **12**, 42099–42108.
78 D.-S. Hou, L. Zheng, D.-P. Sun, X. Zhou, J.-L. Zhu and W.-M. Han, *Liq. Cryst.*, 2022, **49**, 201–208.
79 W. Hu, J. Sun, Q. Wang, L. Zhang, X. Yuan, F. Chen, K. Li, Z. Miao, D. Yang and H. Yu, *et al.*, *Adv. Funct. Mater.*, 2020, **30**, 2004610.
80 T. Guin, B. A. Kowalski, R. Rao, A. D. Auguste, C. A. Grabowski, P. F. Lloyd, V. P. Tondiglia, B. Maruyama, R. A. Vaia and T. J. White, *ACS Appl. Mater. Interfaces*, 2018, **10**, 1187–1194.
81 J. M. Haberl, A. Sánchez-Ferrer, A. M. Mihut, H. Dietsch, A. M. Hirt and R. Mezzenga, *Adv. Mater.*, 2013, **25**, 1787–1791.
82 G. A. Shandryuk, E. V. Matukhina, R. B. Vasil'Ev, A. Rebrov, G. N. Bondarenko, A. S. Merekalov, A. M. Gas'kov and R. V. Talroze, *Macromolecules*, 2008, **41**, 2178–2185.
83 C. J. Camargo, H. Campanella, J. E. Marshall, N. Torras, K. Zinoviev, E. M. Terentjev and J. Esteve, *J. Micromech. Microeng.*, 2012, **22**, 75009.
84 T. Kato, Y. Hirai, S. Nakaso and M. Moriyama, *Chem. Soc. Rev.*, 2007, **36**, 1857–1867.
85 S. Bi, H. Peng, S. Long, M. Ni, Y. Liao, Y. Yang, Z. Xue and X. Xie, *Soft Matter*, 2013, **9**, 7718–7725.
86 N. M. Sangeetha and U. Maitra, *Chem. Soc. Rev.*, 2005, **34**, 821–836.
87 N. Mizoshita, Y. Suzuki, K. Kishimoto, K. Hanabusa and T. Kato, *J. Mater. Chem.*, 2002, **12**, 2197–2201.
88 N. Mizoshita, K. Hanabusa and T. Kato, *Adv. Funct. Mater.*, 2003, **13**, 313–317.
89 V. Sridurai, M. Mathews, C. V. Yelamaggad and G. G. Nair, *ACS Appl. Mater. Interfaces*, 2017, **9**, 39569–39575.
90 Z. Chen, C. Bishop, E. Thoms, H. Bock, M. D. Ediger, R. Richert and L. Yu, *Chem. Mater.*, 2021, **33**, 4757–4764.
91 A. J. Cruz-Cabeza, N. Feeder and R. J. Davey, *Commun. Chem.*, 2020, **3**, 142.
92 S. H. Chen, *J. Soc. Inf. Disp.*, 2004, **12**, 205–211.
93 S. H. Chen, D. Katsis, A. W. Schmid, J. C. Mastrangelo, T. Tsutsui and T. N. Blanton, *Nature*, 1999, **397**, 506–508.
94 A. Gujral, J. Gómez, J. Jiang, C. Huang, K. A. O'Hara, M. F. Toney, M. L. Chabinyc, L. Yu and M. D. Ediger, *Chem. Mater.*, 2017, **29**, 849–858.
95 A. Gujral, L. Yu and M. D. Ediger, *Curr. Opin. Solid State Mater. Sci.*, 2017, 1–9.
96 A. Gujral, S. Ruan, M. F. Toney, H. Bock, L. Yu and M. D. Ediger, *Chem. Mater.*, 2017, **29**, 9110–9119.
97 C. Bishop, Z. Chen, M. F. Toney, H. Bock, L. Yu and M. D. Ediger, *J. Phys. Chem. B*, 2021, **125**, 2761–2770.
98 K. Bagchi, A. Gujral, M. F. Toney and M. D. Ediger, *Soft Matter*, 2019, **15**, 7590–7595.
99 M. E. Fiori, K. Bagchi, M. F. Toney and M. D. Ediger, *Proc. Natl. Acad. Sci. U. S. A.*, 2021, **118**, e2111988118.
100 C. Bishop, J. L. Thelen, E. Gann, M. F. Toney, L. Yu, D. M. DeLongchamp and M. D. Ediger, *Proc. Natl. Acad. Sci. U. S. A.*, 2019, **116**, 21421–21426.
101 M. D. Ediger, *J. Chem. Phys.*, 2017, **147**, 210901.
102 S. S. Dalal, D. M. Walters, I. Lyubimov, J. J. de Pablo and M. D. Ediger, *Proc. Natl. Acad. Sci. U. S. A.*, 2015, **112**, 4227–4232.
103 C. W. Brian and L. Yu, *J. Phys. Chem. A*, 2013, **117**, 13303–13309.
104 X. Li, T. Yanagimachi, C. Bishop, C. Smith, M. Dolejsi, H. Xie, K. Kurihara and P. F. Nealey, *Soft Matter*, 2018, **14**, 7569–7577.
105 R. Ruiz, H. Kang, F. A. Detcheverry, E. Dobisz, D. S. Kercher, T. R. Albrecht, J. J. de Pablo and P. F. Nealey, *Science*, 2008, **321**, 936–939.
106 M. Park, C. Harrison, P. M. Chaikin, R. A. Register and D. H. Adamson, *Science*, 1997, **276**, 1401–1404.
107 T. Thurn-Albrecht, J. Schotter, G. A. Kastle, N. Emley, T. Shibauchi, L. Krusin-Elbaum, K. Guarini, C. T. Black, M. T. Tuominen and T. P. Russell, *Science*, 2000, **290**, 2126–2129.
108 C. Park, J. Yoon and E. L. Thomas, *Polymer*, 2003, **44**, 6725–6760.
109 Q. Chen, S. C. Bae and S. Granick, *Nature*, 2011, **469**, 381–384.
110 T. Deng, C. Chen, C. Honeker and E. L. Thomas, *Polymer*, 2003, **44**, 6549–6553.
111 C. Zhou, T. Segal-Peretz, M. E. Oruc, H. S. Suh, G. Wu and P. F. Nealey, *Adv. Funct. Mater.*, 2017, **27**, 1701756.
112 S.-M. Park, M. P. Stoykovich, R. Ruiz, Y. Zhang, C. T. Black and P. F. Nealey, *Adv. Mater.*, 2007, **19**, 607–611.
113 C. Sinturel, F. S. Bates and M. A. Hillmyer, *ACS Macro Lett.*, 2015, **4**, 1044–1050.
114 X. Xu, J. Wang, Y. Liu and D. Luo, *Adv. Photonics Nexus*, 2023, **2**, 26004.
115 A. C. Balazs, T. Emrick and T. P. Russell, *Science*, 2006, **314**, 1107–1110.
116 S. K. Kumar, B. C. Benicewicz, R. A. Vaia and K. I. Winey, *Macromolecules*, 2017, **50**, 714–731.
117 M. Moniruzzaman and K. I. Winey, *Macromolecules*, 2006, **39**, 5194–5205.
118 S. K. Kumar and R. Krishnamoorti, *Annu. Rev. Chem. Biomol. Eng.*, 2010, **1**, 37–58.
119 M. A. Gharbi, S. Manet, J. Lhermitte, S. Brown, J. Milette, V. Toader, M. Sutton and L. Reven, *ACS Nano*, 2016, **10**, 3410–3415.
120 M. Ravnik, G. P. Alexander, J. M. Yeomans and S. Žumer, *Proc. Natl. Acad. Sci. U. S. A.*, 2011, **108**, 5188–5192.
121 V. Lubchenko and P. G. Wolynes, *Annu. Rev. Phys. Chem.*, 2007, **58**, 235–266.
122 P. G. Wolynes, *Proc. Natl. Acad. Sci. U. S. A.*, 2009, **106**, 1353–1358.
123 O. Narayanaswamy, *J. Am. Ceram. Soc.*, 1971, **54**, 491–498.
124 N. Schupper, Y. Rabin and M. Rosenbluh, *Macromolecules*, 2008, **41**, 3983–3994.

125 J. Jumper, R. Evans, A. Pritzel, T. Green, M. Figurnov, O. Ronneberger, K. Tunyasuvunakool, R. Bates, A. Žídek and A. Potapenko, *et al.*, *Nature*, 2021, **596**, 583–589.
126 A. Vriza, H. Chan and J. Xu, *Chem. Mater.*, 2023, **35**, 3046–3056.
127 C. Wang, Y.-J. Kim, A. Vriza, R. Batra, A. Baskaran, N. Shan, N. Li, P. Darancet, L. Ward and Y. Liu, *et al.*, *Nat. Commun.*, 2025, **16**, 1498.
128 A. Nyayachavadi, C. Wang, A. Vriza, Y. Wang, G. Ma, M. Mooney, G. T. Mason, A. Hu, Y. Liu and X. Gu, *et al.*, *Adv. Funct. Mater.*, 2024, **34**, 2403612.
129 A. Piven, D. Darmoroz, E. Skorb and T. Orlova, *Soft Matter*, 2024, **20**, 1380–1391.
130 Y. Cao, H. Yu, N. L. Abbott and V. M. Zavala, *ACS Sens.*, 2018, **3**, 2237–2245.
131 S. R. Johnson and P. C. Jurs, *Chem. Mater.*, 1999, **11**, 1007–1023.
132 D. Antanasijević, J. Antanasijević, V. Pocajt and G. Uščumlić, *RSC Adv.*, 2016, **6**, 99676–99684.
133 C.-H. Chen, K. Tanaka and K. Funatsu, *Mol. Inform.*, 2019, **38**, 1800095.